J. Shanghai Jiao Tong Univ. (Sci.), 2017, 22(3): 343-348
DOI: 10.1007/s12204-017-1841-5

A Generalized Self-Consistent Model for Interfacial Debonding Behavior of Fiber Reinforced Rubber Matrix Sealing Composites

ZHANG Bin[1,2*] (张　斌), *YU Xiaoming*[1] (宇晓明), *GU Boqin*[3] (顾伯勤)
(1. School of Mechanical Engineering, Changshu Institute of Technology, Changshu 215500, Jiangsu, China; 2. Jiangsu Key Laboratory of Recycling and Reuse Technology for Mechanical and Electronic Products, Changshu Institute of Technology, Changshu 215500, Jiangsu, China; 3. College of Mechanical and Power Engineering, Nanjing Tech University, Nanjing 211816, China)

Abstract: This paper presents an experimental and numerical study of short-fiber-reinforced rubber matrix sealing composites (SFRC). The transverse tensile stress-strain curves of SFRC are obtained by experiments. Based on the generalized self-consistent method, a representative volume element (RVE) model is established, and the cohesive zone model is employed to investigate the interfacial failure behavior. The effect of interphase properties on the interfacial debonding behavior of SFRC is numerically investigated. The results indicate that an interphase thickness of 0.3 μm and an interphase elastic modulus of about 502 MPa are optimal to restrain the initiation of the interfacial debonding. The interfacial debonding of SFRC mainly occurs between the matrix/interphase interface, which agrees well with results by scanning electron microscope (SEM).
Key words: fiber, rubber, composites, interphase, interfacial debonding
CLC number: TB 332　　**Document code:** A

0 Introduction

Short-fiber-reinforced rubber matrix sealing composites (SFRC), such as aramid, glass and carbon fiber reinforced rubber sheet, are widely used in petroleum, chemical, textile, electrical and mechanical industries. Fibers or particles embedded in a rubber matrix can effectively improve the comprehensive performance of materials, for example, high strength, fatigue resistance and corrosion resistance. Engineering practice confirms that these kinds of composites have good applicability over recent years[1].

Interfacial debonding is an important factor affecting the mechanical behavior of composites. Zhang et al.[2] studied the effect of the interfacial properties on the failure behavior of short fiber reinforced rubber composites. The results indicate that a good interfacial strength and a suitable interphase modulus can enhance the ductility and strength of composites. Vaughan et al.[3] presented a micromechanics damage model to examine the effect of fiber-matrix debonding and thermal residual stress on the transverse damage behavior of a unidirectional carbon fiber reinforced epoxy composite. It is found that for a strong fiber-matrix interface the presence of thermal residual stress is effective in suppressing fiber-matrix debonding and improving overall transverse strength. Hobbiebrunken et al.[4] and Canal et al.[5] presented experimental evidence of interfacial debonding in composite failure by in-suit observation. It is found that the failure behavior of composite materials is dependant upon numerous contributing factors, such as constituent properties and interfacial properties. The performance of composites such as fiber reinforced resin matrix and metal matrix can be accurately predicted by mesoscopic numerical models[6-7]. However, the rubber matrix composites make its mechanical behavior more complicated due to special performances of rubber (small modulus, large deformation, hyperelasticity, etc.), which leads to relatively less research work reported[8-9].

Two-phase composite materials have been exploited for decades in engineering design, and they have been proved having great applicability and high performance. However, it has been suggested that some materials previously considered to be two-phase com-

Received date: 2016-01-28
Foundation item: the National Natural Science Foundation of China (No. 51375223), Open Research Fund by Jiangsu Key Laboratory of Recycling and Reuse Technology for Mechanical and Electronic Products (No. RRME-KF1611), and Scientific Research Foundation for Advanced Talents (No. XZ1517)
∗**E-mail:** drzhbin@163.com

posites are better described in terms of a third phase model[10-11]. Interphase performance is considered to be a key factor in the study of comprehensive mechanical performance of composites. Zhu et al.[12] established a micromechanical model of short-fiber-reinforced elastomer matrix composite. The time-dependent tensile stress distribution on the fiber and the time-dependent shear stress distribution in the matrix and interphase are derived. Yuan et al.[13] established the finite element model of interfacial reaction layer and analyzed the influence of interphase reaction on interfacial shear strength of composites. Zhang et al.[14] investigated interphase effect on the strengthening behavior of particle-reinforced metal matrix composites. The numerical results indicate that hard and soft interphases result in the increase and significant decrease of the strength of composite, respectively.

The purpose of this work is to investigate the effect of interphase properties on the interfacial debonding behavior of SFRC. The transverse tensile stress-strain curves of SFRC are obtained by experiments. A generalized self-consistent finite element model (FEM) under transverse tensile load is established, where the cohesive elements are embedded in the fiber/interphase (FI) and matrix/interphase (MI) interfaces, respectively. In the modeling strategy, the initial strain and location of the interfacial debonding with different interphase elastic modulus and thickness are obtained, and then the optimum interphase properties are determined.

1 Computational Micromechanics Model

1.1 Generalized Self-Consistent Method

The generalized self-consistent method is a sophisticated micromechanics approach[15]. Different from the other micromechanics methods (self-consistent, differential and Mori-Tanaka methods) based on the two-phase model[16], the generalized self-consistent method is based on a three-phase model: an inclusion is embedded in a finite matrix, which in turn is embedded in an infinite composite with the as-yet-unknown effective moduli. The generalized self-consistent method provides accurate predictions for extreme types of inclusions (i.e. voids and rigid inclusions), and the method also gives the correct asymptotic behavior of composites with high volume fraction of the inclusion. It is shown that the results of the generalized self-consistent method have excellent agreement with the experimental data[17].

1.2 Representative Volume Element Model

In this paper, the representative volume element (RVE) model is established using the generalized self-consistent method, as shown in Fig. 1(a). It is composed of the fiber, rubber matrix and effective composites. The property of the effective composites is

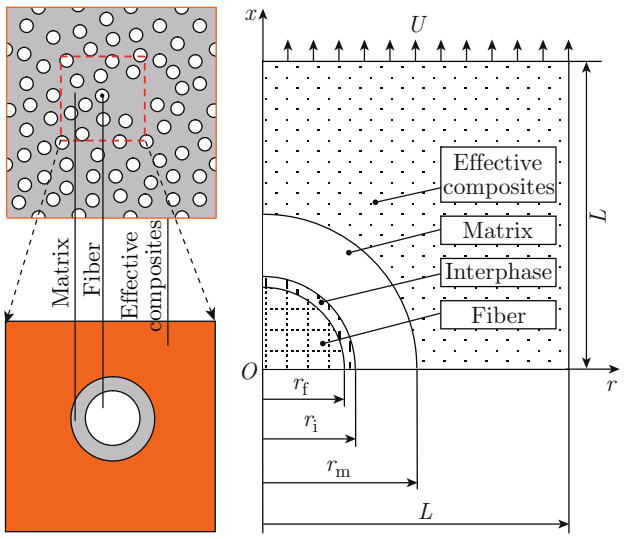

(a) Generalized self-consistent model (b) Plane RVE model and coordinate system

Fig. 1 The RVE model

equal to that of the global composites. In order to reduce the computational effort, only a plane RVE is modeled using periodic boundary conditions. The coordinate system is shown in Fig. 1(b) where L is the outer size of the RVE. r_f, r_i and r_m are the radius of the fiber, interphase and matrix, respectively. The fiber has constant radius of 7.5 μm. González et al.[18] indicated that if $L/r_\mathrm{m} \geqslant 5$, the external boundary conditions have no influence on the deformation of the RVE. Therefore, $L/r_\mathrm{m} = 5$ is chosen. r_m is fixed and r_f is changed to obtain various fiber volume fractions which can be calculated by $\nu_\mathrm{f} = r_\mathrm{f}^2/r_\mathrm{m}^2$. Only one quarter of the physical model is required in the analysis due to the axial symmetry.

For the present RVE model, the boundary conditions include

$$\left.\begin{aligned} u_r &= 0 \quad \text{at } r = 0 \\ u_x &= 0 \quad \text{at } x = 0 \\ u_x &= U \quad \text{at } x = L \end{aligned}\right\}, \tag{1}$$

where u_r and u_x are the displacements in the r and x directions, respectively, and U is the displacement at $x = L$. During deformation, the boundary of the model is enforced to hold straight at $r = L$.

A finite element model is created using the package ABAQUS/Standard (2010) and the corresponding finite element meshes are shown in Fig. 2. The fiber, interphase and effective composites are modeled using 4 node bilinear plane strain quadrilateral elements (CPE4R). The rubber matrix is regarded as a hyperelastic material, which requires the use of elements with hybrid formulation. The elements chosen in this model are the linear quadrilateral hybrid elements (CPE4H), with a mesh sufficiently fine to provide at least two elements between two adjacent fibers. The cohesive zone

model is employed to simulate the interfacial debonding between the fiber/interphase (FI) interface and the matrix/interphase (MI) interfaces, respectively. A typical model comprises approximately 5 000 elements and the model with finer meshes (up to 10 000 elements) provides the same results.

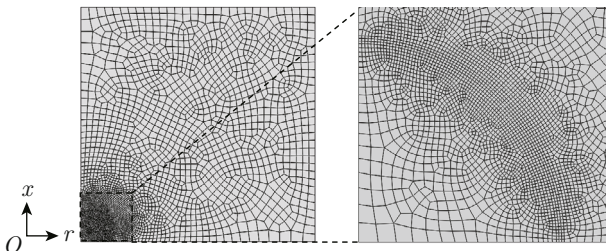

(a) Whole model for calculation (b) Partially enlarged

Fig. 2 Finite element meshes

1.3 Cohesive Zone Model

The cohesive zone model employed to describe the damage of the interface refers to our previous research, as shown in Fig. 3[2]. The mechanical behavior of these elements is expressed in terms of a traction-separation law which relates the displacement jump across the interface with the traction vector acting upon it. An element size of nearly $0.03\,r_{\mathrm{f}}$, where r_{f} is the fiber radius, is used in a vicinity of the interface. The initial response is linear in absence of damage, and therefore, the traction-separation law can be written as

$$\left.\begin{aligned} t_{\mathrm{n}} &= K\delta_{\mathrm{n}} \\ t_{\mathrm{s}} &= K\delta_{\mathrm{s}} \end{aligned}\right\}, \tag{2}$$

where t_{n}, t_{s}, δ_{n} and δ_{s} stand for the normal and tangential tractions and displacement jumps across the interface respectively. The initial response is linear in absence of damage with an elastic stiffness of K. An elastic stiffness $K = 10^5\,\mathrm{GPa/m}$ is selected for the interface, which is large enough to ensure the displacement continuity at the interface and to avoid any modification of the stress field around the fibers in the absence of damage[3].

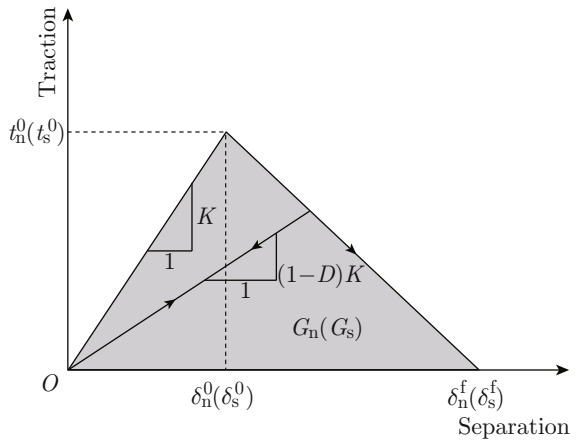

Fig. 3 Traction-separation law of the cohesive zone model

Damage is assumed to be initiated when the maximum nominal stress ratio reaches one of the values given by the following equation

$$\max\left\{\frac{\langle t_{\mathrm{n}}\rangle}{t_{\mathrm{n}}^0}, \frac{t_{\mathrm{s}}}{t_{\mathrm{s}}^0}\right\} = 1, \tag{3}$$

where $\langle\rangle$ are the Macaulay brackets, which return the argument if positive and zero otherwise, to impede the development of damage when the interface is under compression. t_{n}^0 and t_{s}^0 are the interfacial normal and shear strengths. δ_{n}^0 and δ_{s}^0 are the interfacial normal and tangential displacement. G_{n} and G_{s} are the interfacial normal and shear fracture energy. For simplicity, we assumed that t_{n}^0 is equal to t_{s}^0, that is, $t_{\mathrm{n}}^0 = t_{\mathrm{s}}^0$. Once damage begins, the traction stress is reduced depending on the interface damage parameter D, which evolves from 0 (in the absence of damage) to 1 (at ultimate failure), as shown in Fig. 3. The displacement at failure ($\delta_{\mathrm{n}}^{\mathrm{f}}$ or $\delta_{\mathrm{s}}^{\mathrm{f}}$) is determined by the fracture energy G, which corresponds to the area under the traction-separation curve.

The values of the cohesive parameters are as follows[3,19]: $K = 10^5\,\mathrm{GPa/m}$, $t_{\mathrm{n}}^0 = t_{\mathrm{s}}^0 = 2.1\,\mathrm{MPa}$ and $G = 0.1\,\mathrm{J/m^2}$.

2 Results and Discussion

2.1 Properties of Constituent Material

The experimental transverse tensile stress-strain curve of SFRC with 15% fiber volume fraction is shown in Fig. 4(a). According to Chinese national standard GB/T 9129—2003, the compressive stress of rubber gasket is needed to reach 7 MPa. It can be seen that the experimental results meet the specified index.

The experimental tensile stress-strain curve of pure rubber is shown in Fig. 4(b). It is a convenient way to define the material model of hyperelastic composites by providing rubber uniaxial test data to ABAQUS. The

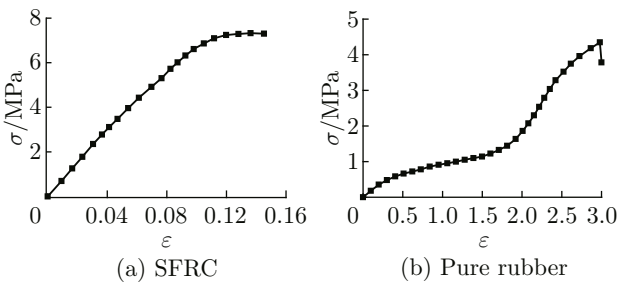

(a) SFRC (b) Pure rubber

Fig. 4 Transverse tensile stress-strain curves

type of strain potential energy can be determined according to the contrast diagrams of stress-strain curves given in ABAQUS. The rubber matrix is modeled as a hyperelastic material. A Mooney-Rivlin model introduced by Melvin Mooney and Ronald Rivlin[20], is used, where the strain energy density function $\boldsymbol{W}$ is a linear combination of two invariants of the left Cauchy-Green deformation tensor. The strain energy density function for an incompressible Mooney-Rivlin material is as follows

$$\boldsymbol{W} = C_1(\boldsymbol{I}_1 - 3) + C_2(\boldsymbol{I}_2 - 3), \tag{4}$$

where C_1 and C_2 are empirically determined material constants, and $\boldsymbol{I}_1$ and $\boldsymbol{I}_2$ are the first and the second invariants of the deviatoric component of the left Cauchy-Green deformation tensor. The computed parameters C_1 and C_2 are 0.128 MPa and 0.198 MPa, respectively.

The aramid fiber is modeled as a linear elastic, homogeneous isotropic material. The elastic modulus and Poisson ratio of the aramid fiber are $E_\mathrm{f} = 136$ GPa and $v_\mathrm{f} = 0.2$, respectively[21].

The interphase property $P_\mathrm{i}(r)$ varied with radius is given as[22-24]

$$\frac{P_\mathrm{i}(r)}{P_\mathrm{m}} = 1 - A\left[\frac{r_\mathrm{i} - r}{r_\mathrm{i} - r_\mathrm{f}}\right]^Q, \tag{5}$$

where $P_\mathrm{i}(r)$ is the interphase property, which can be the elastic modulus, shear modulus, Poisson's ratio, and so on. P_m is the matrix property, r is the radius, the subscripts i, and f refer to interphase and fiber, respectively, and A and Q are material parameters. The parameter A is called the adhesion factor, and $A = [P_\mathrm{m} - P_\mathrm{i}(r_\mathrm{f})]/P_\mathrm{m}$.

In order to simplify the problem, the interphase properties are regard as the average values of the gradient distribution parameters, and then the average interphase properties P_i is given as:

$$P_\mathrm{i} = \frac{1}{(r_\mathrm{i} - r_\mathrm{f})}\int_{r_\mathrm{f}}^{r_\mathrm{i}} P_\mathrm{i}(r)\mathrm{d}r. \tag{6}$$

The interfacial adhesion is usually poor between the aramid fiber and rubber matrix, which restricts the mechanical properties of the composites. The reason is that the surface of aramid fiber is smooth, and lack of polar groups and chemical activity. In general, epoxy resin coating is used as the surface treatment method of the aramid fiber[19]. Thus, the interphase elastic modulus varies between $E_\mathrm{e} = 3$ GPa (fiber coated with the epoxy resin) and $E_\mathrm{m} = 2$ MPa (rubber matrix). The gradient distribution and isotropy of interphase elastic modulus is shown in Fig. 5(a) and Fig. 5(b), respectively. In this paper, the average moduli of interphase (E_i) are 502, 752, 1 001, 1 501 and 2 000 MPa, respectively, which is calculated by different Q.

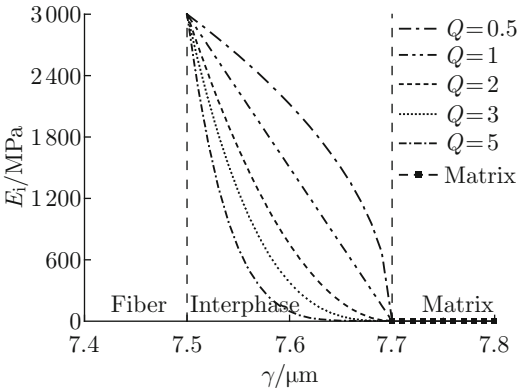

(a) Gradient interphase elastic modulus

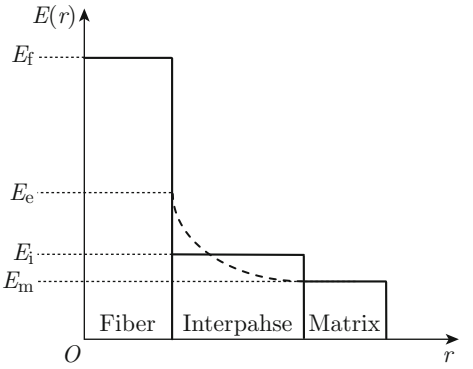

(b) Average interphase elastic modulus

Fig. 5 The distribution of interphase elastic modulus

2.2 Interphase Effect on Initial Strain of Interfacial Debonding

In order to investigate the influence of interphase properties on interfacial debonding behavior of SFRC with different interphase elastic moduli E_i and interphase thicknesses t, the numerical analysis of a finite element model with 15% fiber volume fraction are conducted. Figure 6 illustrates the effect of various E_i and t on the initial strain of the interfacial debonding (ε_0). The interphase thicknesses t is regarded as 0.1,

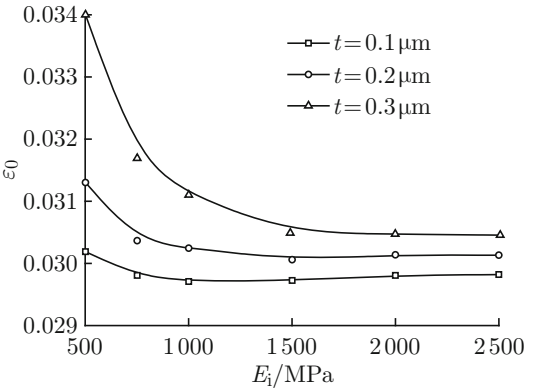

Fig. 6 The initial strain of the interfacial debonding (ε_0) of SFRC with 15% fiber volume fraction

0.2 and 0.3 μm[21]. The results show that ε_0 increases with the increase of t, and it has the maximum value with $t = 0.3\,\mu m$ and $E_i = 502\,MPa$. It can also be seen that ε_0 remains stable when E_i is larger than 1 500 MPa. Therefore, in order to restrain the initiation of the interfacial debonding of SFRC, an interphase thickness of about 0.3 μm and an interphase elastic modulus of about 502 MPa are optimal.

2.3 Interphase Effect on Initial Location of Interfacial Debonding

Figure 7 presents photos of cross section of aramid reinforced rubber matrix composites imaged by scanning electron microscope (SEM). Figure 7(a) shows that the surfaces of the aramid fibers without treatment are very smooth, and there are only a few rubber particles adhering on the fiber surfaces. After surface treatments, the adhesion effect between fiber and rubber matrix is obviously improved. Figure 7(b) shows there are a large number of rubber particles adhering on the aramid fibers and interfacial debonding occurs near the matrix/interphase (MI) interfaces.

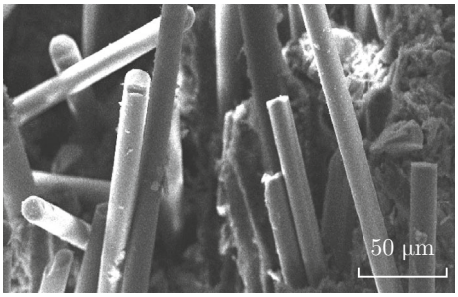

(a) Without surface treatment

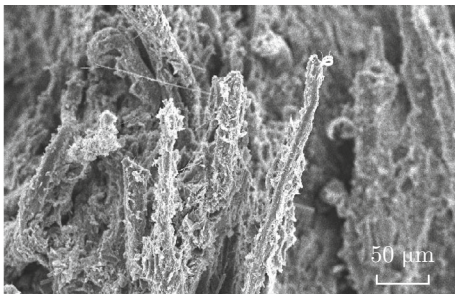

(b) With surface treatment

Fig. 7 SEM photos of cross tensile section of aramid fiber reinforced rubber composites

The initial location of the interfacial debonding of SFRC with $t = 0.3\,\mu m$ and $E_i = 502\,MPa$ is shown in Fig. 8. It can be also obtained that t and E_i have no effects on the initial location of the interfacial debonding with other computational models. The interfacial initial debonding mainly appears at the location between matrix/interphase interfaces at the pole point, where $\theta = 90°$. Therefore, the predicted results agree well with experimental results observed by SEM.

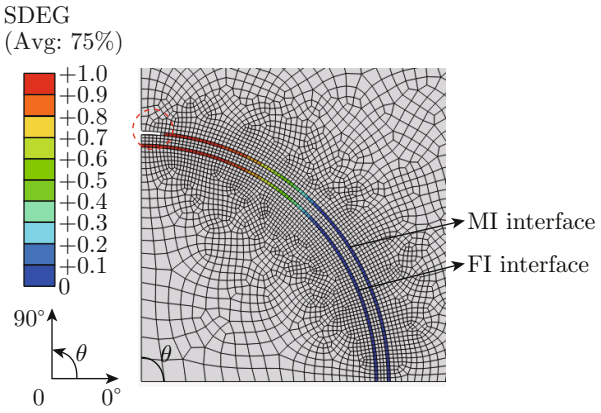

Fig. 8 The initial location of the interfacial debonding of SFRC

3 Conclusion

The transverse tensile stress-strain curves of aramid fiber reinforced rubber sealing composites (SFRC) are obtained by experiments. The interfacial debonding behavior of SFRC is observed by SEM. A 2D finite element model based on the generalized self-consistent method is employed to investigate the interfacial failure behavior. The effects of interphase elastic modulus E_i and interphase thickness t on the initial strain of interfacial debonding (ε_0) are investigated. The results indicate that E_i of about 502 MPa and t of about 0.3 μm are optimal to restrain the initiation of the interfacial debonding. The initial debonding location of SFRC is investigated. The results show that E_i and t have no effects on the initial location of the interfacial debonding. The interfacial debonding mainly occurs between the matrix/interphase interface, which agrees well with experimental results.

References

[1] TIAN M, SU L, CAI W T, et al. Mechanical properties and reinforcement mechanisms of hydrogenated acrylonitrile butadiene rubber composites containing fibrillar silicate nanofibers and short aramid microfibers [J]. *Journal of Applied Polymer Science*, 2011, **120**(3): 1439-1447.

[2] ZHANG B, GU B Q, YU X M. Failure behavior of resorcinol-formaldehyde latex coated aramid short-fiber-reinforced rubber sealing under transverse tension [J]. *Journal of Applied Polymer Science*, 2015, **132**: 41672. DOI: 10.1002/app.41672 (published online).

[3] VAUGHAN T J, MCCARTHY C T. Micromechanical modelling of the transverse damage behaviour in fibre reinforced composites [J]. *Composites Science and Technology*, 2011, **71**(3): 388-396.

[4] HOBBIEBRUNKEN T, HOJO M, ADACHI T, et al. Evaluation of interfacial strength in CF/epoxies using FEM and in-situ experiments [J]. *Composites Part*

A: Applied Science and Manufacturing, 2006, **37**(12): 2248-2256.

[5] CANAL L P, GONZÁLEZ C, SEGURADO J, et al. Intraply fracture of fiber-reinforced composites: Microscopic mechanisms and modeling [J]. *Composites Science and Technology*, 2012, **72**(11): 1223-1232.

[6] ZHANG Y Y, ZHU S W, LIU Y, et al. The mechanical and tribological properties of nitric acid-treated carbon fiber-reinforced polyoxymethylene composites [J]. *Journal of Applied Polymer Science*, 2015, **132**: 41812. DIO: 10.1002/app.41812 (published online).

[7] STARINK M J, SYNGELLAKIS S. Shear lag models for discontinuous composites: Fibre end stresses and weak interface layers [J]. *Materials Science and Engineering: A*, 1999, **270**(2): 270-277.

[8] MORALEDA J, SEGURADO J, LLORCA J. Finite deformation of incompressible fiber-reinforced elastomers: A computational micromechanics approach [J]. *Journal of the Mechanics and Physics of Solids*, 2009, **57**(9): 1596-1613.

[9] LI X, XIA Y, LI Z, et al. Three-dimensional numerical simulations on the hyperelastic behavior of carbon-black particle filled rubbers under moderate finite deformation [J]. *Computational Materials Science*, 2012, **55**: 157-165.

[10] AFONSO J C, RANALLI G. Elastic properties of three-phase composites: Analytical model based on the modified shear-lag model and the method of cells [J]. *Composites Science and Technology*, 2005, **65**(7): 1264-1275.

[11] WANG X Q, ZHAO W T, FANG B, et al. Micromechanical analysis of long fiber-reinforced composites with nanoparticle incorporation into the interphase region [J]. *Journal of Applied Polymer Science*, 2015, **132**: 41573. DOI: 10.1002/app.41573 (published online).

[12] ZHU D S, GU B Q, CHEN Y. Micromechanical model of stress distribution and transfer in short-fiber-reinforced elastomer matrix composite [J]. *Journal of Computational and Theoretical Nanoscience*, 2008, **5**(8): 1546-1550.

[13] YUAN M N, YANY Y Q, HUANG B, et al. Effect of interface reaction on interface shear strength of SiC fiber reinforced titanium matrix composites [J]. *Rare Metal Materials and Engineering*, 2009, **38**(8): 1321-1324.

[14] ZHANG W X, LI L X, WANG T J. Interphase effect on the strengthening behavior of particle-reinforced metal matrix composites [J]. *Computational Materials Science*, 2007, **41**(2): 145-155.

[15] JIANG C P, TONG Z H, CHEUNG Y K. A generalized self-consistent method for piezoelectric fiber reinforced composites under antiplane shear [J]. *Mechanics of Materials*, 2001, **33**(5): 295-308.

[16] ZHANG B, GU B Q, YU X M. Prediction method for longitudinal tensile-modulus of aramid short-fiber-reinforced rubber sealing composites [J]. *Journal of Shanghai Jiao Tong University*, 2015, **49**(1): 96-100 (in Chinese).

[17] HUANG Y, HU K X, CHANDRA A. A generalized self-consistent mechanics method for microcracked solids [J]. *Journal of the Mechanics and Physics of Solids*, 1994, **42**(8): 1273-1291.

[18] GONZÁLEZ C, LLORCA J. Mechanical behavior of unidirectional fiber-reinforced polymers under transverse compression: Microscopic mechanisms and modeling [J]. *Composites Science and Technology*, 2007, **67**(13): 2795-2806.

[19] SA R, YAN Y, WEI Z H, et al. Surface modification of aramid fibers by bio-inspired poly(dopamine) and epoxy functionalized silane grafting [J]. *ACS Applied Materials and Interfaces*, 2014, **6**(23): 21730-21738.

[20] JIMÉNEZ F L, PELLEGRINO S. Constitutive modeling of fiber composites with a soft hyperelastic matrix [J]. *International Journal of Solids and Structures*, 2012, **49**(3): 635-647.

[21] YU X M, GU B Q, ZHANG B. Effects of short fiber tip geometry and inhomogeneous interphase on the stress distribution of rubber matrix sealing composites [J]. *Journal of Applied Polymer Science*, 2015, **132**: 41638. DOI: 10.1002/app.41638 (published online).

[22] SHEN L X, LI J. Effective elastic moduli of composites reinforced by particle or fiber with an inhomogeneous interphase [J]. *International Journal of Solids and Structures*, 2003, **40**(6): 1393-1409.

[23] KIRITSI C C, ANIFANTIS N K. Load carrying characteristics of short fiber composites containing a heterogeneous interphase region [J]. *Computational Materials Science*, 2001, **20**(1): 86-97.

[24] NGABONZIZA Y, LI J, BARRY C F. Electrical conductivity and mechanical properties of multiwalled carbon nanotube-reinforced polypropylene nanocomposites [J]. *Acta Mechanica*, 2011, **220**(1): 289-298.